

Alloying and magnetic disordering effects on phase stability of Co_2YGa (*Y*=Cr, V, and Ni) alloys: A first-principles study

Chun-Mei Li(李春梅), Shun-Jie Yang(杨顺杰), and Jin-Ping Zhou(周金萍)
Citation: Chin. Phys. B, 2022, 31 (**5**): 056105. DOI: 10.1088/1674-1056/ac3986
Journal homepage: http://cpb.iphy.ac.cn; http://iopscience.iop.org/cpb

What follows is a list of articles you may be interested in

First-principles study of stability of point defects and their effects on electronic properties of GaAs/AlGaAs superlattice

Shan Feng(冯山), Ming Jiang(姜明), Qi-Hang Qiu(邱启航), Xiang-Hua Peng(彭祥花), Hai-Yan Xiao(肖海燕), Zi-Jiang Liu(刘子江), Xiao-Tao Zu(祖小涛), and Liang Qiao(乔梁)
Chin. Phys. B, 2022, 31 (**3**): 036104. DOI: 10.1088/1674-1056/ac16cb

A new direct band gap silicon allotrope o-Si32

Xin-Chao Yang(杨鑫超), Qun Wei(魏群), Mei-Guang Zhang(张美光), Ming-Wei Hu(胡明玮), Lin-Qian Li(李林茜), and Xuan-Min Zhu(朱轩民)
Chin. Phys. B, 2022, 31 (**2**): 026104. DOI: 10.1088/1674-1056/ac11db

First-principles study of two new boron nitride structures: C12-BN and O16-BN

Hao Wang(王皓), Yaru Yin(殷亚茹), Xiong Yang(杨雄), Yanrui Guo(郭艳蕊), Ying Zhang(张颖), Huiyu Yan(严慧羽), Ying Wang(王莹), and Ping Huai(怀平)
Chin. Phys. B, 2022, 31 (**2**): 026102. DOI: 10.1088/1674-1056/ac0a69

Effect of structural vacancies on lattice vibration, mechanical, electronic, and thermodynamic properties of Cr5BSi3

Tian-Hui Dong(董天慧), Xu-Dong Zhang(张旭东), Lin-Mei Yang(杨林梅), and Feng Wang(王峰)
Chin. Phys. B, 2022, 31 (**2**): 026101. DOI: 10.1088/1674-1056/ac11e2

Spin and spin-orbit coupling effects in nickel-based superalloys: A first-principles study on Ni3Al doped with Ta/W/Re

Liping Liu(刘立平), Jin Cao(曹晋), Wei Guo(郭伟), and Chongyu Wang(王崇愚)
Chin. Phys. B, 2022, 31 (**1**): 016105. DOI: 10.1088/1674-1056/ac4024

Alloying and magnetic disordering effects on phase stability of Co_2YGa (Y = Cr, V, and Ni) alloys: A first-principles study

Chun-Mei Li(李春梅)[†], Shun-Jie Yang(杨顺杰), and Jin-Ping Zhou(周金萍)

College of Physics Science and Technology, Shenyang Normal University, Shenyang 110034, *China*

(Received 24 June 2021; revised manuscript received 14 October 2021; accepted manuscript online 15 November 2021)

The alloying and magnetic disordering effects on site occupation, elastic property, and phase stability of Co_2YGa (Y = Cr, V, and Ni) shape memory alloys are systematically investigated using the first-principles exact muffin-tin orbitals method. It is shown that with the increasing magnetic disordering degree y, their tetragonal shear elastic constant C' (i.e., $(C_{11}-C_{12})/2$) of the $L2_1$ phase decreases whereas the elastic anisotropy A increases, and upon tetragonal distortions the cubic phase gets more and more unstable. Co_2CrGa and Co_2VGa alloys with $y \geq 0.2$ thus can show the martensitic transformation (MT) from $L2_1$ to $D0_{22}$ as well as Co_2NiGa. In off-stoichiometric alloys, the site preference is controlled by both the alloying and magnetic effects. At the ferromagnetism state, the excessive Ga atoms always tend to take the Y sublattices, whereas the excessive Co atom favor the Y sites when Y = Cr, and the excessive Y atoms prefer the Co sites when Y = Ni. The Ga-deficient Y = V alloys can also occur the MT at the ferromagnetism state by means of Co or V doping, and the MT temperature T_M should increase with their addition. In the corresponding ferromagnetism Y = Cr alloys, nevertheless, with Co or Cr substituting for Ga, the reentrant MT (RMT) from $D0_{22}$ to $L2_1$ is promoted and then T_M for the RMT should decrease. The alloying effect on the MT of these alloys is finally well explained by means of the Jahn–Teller effect at the paramagnetic state. At the ferromagnetism state, it may originate from the competition between the austenite and martensite about their strength of the covalent banding between Co and Ga as well as Y and Ga.

Keywords: first-principles, martensitic transformation, elastic modulus, magnetic ordering, shape memory alloys

PACS: 61.66.Dk, 62.20.de, 63.20.dk, 64.70.K– **DOI:** 10.1088/1674-1056/ac3986

1. Introduction

Several Co_2-based Heusler alloys (with the stoichiometric composition X_2YZ) such as Co–Ni–Ga,[1,2] $Co_2Cr(Ga,Si)$,[3] $Co_2Cr(Al,Si)$,[4] Co–V–Ga,[5–9] and Co–V–Si[10,11] recently have attracted a lot of research due to their extrordinary shape memory effect. This is because they possess the reversible martensitic transformation (MT) from the $L2_1$ phase (face-centered-cubic, fcc, space group $Fm\bar{3}m$) to the so-called $D0_{22}$ phase (body-centered-tetragonal, bct, space group $I4/mmm$), described clearly in Ref. [12] although in some compositions, other related structures, such as the inverse Heusler ($L2_1$)[13,14] and the disordered B_2 cubic phases,[2,15] and the orthorhombic and monoclinic martensite,[16] may also coexist. Among them, $Co_2Cr(Ga,Si)$ alloys can also occur with $L2_1$–$D0_{22}$–$L2_1$ successive transitions upon cooling from the paramagnetic (PM) state to the ferromagnetic (FM) state,[3] showing an abnormal behavior of reentrant martensitic transformation (RMT) from $D0_{22}$ to $L2_1$. Some PM state of Co–V–Si alloys can even exhibit their shape memory effect up to about 700 °C,[10] higher than the MT temperatures (T_M) measured in most shape memory alloys. Compared to the traditional Ni–Mn–Ga alloys, these Co_2-based shape memory alloys also possess relatively good mechanical property, processability, and corrosion resistance.[10,17] They therefore have a broad prospect for applications in the area of biomedicine, automotive, aerospace, and chemistry industry.

Similar to the traditional Ni–Mn–Ga alloys, the reversible MT behavior of these Co_2-based shape memory alloys is highly composition-dependent. With respect to the composition, T_M changes from 250 K to 500 K in Co–V–Ga alloys,[5,6] and in Co–Ni–Ga alloys it even varies from 100 K up to 800 K.[18,19] The phenomenon of RMT from $D0_{22}$ to $L2_1$ was clearly observed only in some $Co_2Cr(Ga,Si)$ alloys,[3,20] T_M for the normal MT of $L2_1$–$D0_{22}$ and that for the RMT change oppositely against the composition. Correspondingly, in these alloys the entropy difference between the $L2_1$ and $D0_{22}$ phases has been confirmed to be positive during the RMT but negative in the normal MT,[3,20] and during the two phase transitions, an inverse temperature dependence of superelastic stress[12,20] as well as electric resistivity[3] was also found in $Co_{49.7}Cr_{28.3}Ga_{11}Si_{11}$ alloy. Exploring the alloying effect on the thermodynamic properties and phase stabilities of these Co_2YGa (Y = Cr, V, and Ni) Heusler alloys and then trying to find out their physical mechanisms are critical to design them with good shape memory effect. However, until now, their true story is still not deeply understood.

There are several plausible quantities to connect the composition and T_M of Ni–Mn–Ga alloys, such as the number

[†]Corresponding author. E-mail: cmli@synu.edu.cn

© 2022 Chinese Physical Society and IOP Publishing Ltd

of valence electrons per atom (e/a),[21–23] the energy difference between the cubic austenite and the tetragonal martensite (ΔE^{AM}),[24] the tetragonal shear modulus of the parent phase ($C' = (C_{11} - C_{12})/2$),[25,26] and the tetragonality of the martensite ($|1 - c/a|$).[27,28] Generally, T_{M} increases with the increase of e/a, ΔE^{AM}, and $|1 - c/a|$, whereas decreases with increasing C'. The established correlation between T_{M} and e/a is also followed by the most Co_2YGa (Y = Cr, V, and Ni)-based alloys.[3,6,18,19] Nevertheless, the relationships of $T_{\mathrm{M}} \sim \Delta E^{\mathrm{AM}}$, $T_{\mathrm{M}} \sim |1 - c/a|$, and $T_{\mathrm{M}} \sim C'$ have never been examined. In addition, similar to Ni–Mn–In alloys,[29] the excessive Mn atoms on the In sites are FM coupling with those on their own sites in the $L2_1$ phase, whereas in the tetragonal $D0_{22}$ martensite they turn out to be anti-ferromagnetic (AFM) coupling with each other, in $Co_2Cr(Ga,Si)$ alloys the RMT occurs at the FM state whereas the normal MT happens at the PM state.[3,20] The magnetic ordering therefore may also be associated with the phase stability of these Co_2-based alloys at finite temperatures. Furthermore, the MT from $L2_1$ to tetragonal pase in Ni–Mn–Ga can be traced to the Jahn–Teller distortion and Fermi surface nesting at the electronic structure level.[30,31] This electronic origination as well as the alloying and magnetic ordering effects on the MT also needs to be ascertained in these Co_2-based shape memory alloys.

In this paper, we systematically investigate both the alloying and magnetic disordering effects on the thermodynamic properties and phase stabilities of the $L2_1$ and $D0_{22}$ phases of Co_2YGa (Y = Cr, V, and Ni) Heusler alloys, and then try to find out the physical mechanisms driving their composition-dependent MT. In order to have a better comparison among the three groups of alloys, the other complicated structures are neglected in both the austenite and martensite. Though for the FM Y = Ni alloy, the inverse Heusler structure[13] is also found to be lower than the $L2_1$ structure in energy about 0.23 mRy from our calculations. However, the latter structure corresponds to the ground state of both Y = Cr and V alloys, and the MT of $L2_1$–$D0_{22}$ can be found in Co_2NiGa alloy as well.[13] The rest of the paper is arranged as follows: In Section 2, we describe the first-principles method used and the calculation details. In Section 3, the site occupation, equilibrium properties, elastic property, and phase stability of nine groups of off-stoichiometric alloys as well as the three stoichiometric ones are presented at both the FM and PM states, the alloying and magnetic ordering effects on these properties are explored, and the mechanism driving the composition-dependent MT of these alloys is discussed together with their calculated electronic structure. Finally, we summarize the main results of this work in Section 4.

2. Methods and calculation details

Based on density-functional theory (DFT), the employed first-principles solver is the exact muffin-tin orbitals (EMTO) method,[32–35] in combination with the optimized overlapping muffin-tin approximation for the effective potential[32,36] and the full-charge density technique for the total energy.[35,37] This approach is then suitable to accurately describe the total energy change with respect to anisotropic lattice distortions. In addition, within the EMTO method, the single-electron Kohn–Shan equations are solved by using Green's function technique and the substitutional disorder is treated using the coherent potential approximation (CPA).[38–40] Our main motivation for choosing this method is that it is flexible enough to describe both the atomic disorders and magnetic disorders in the Co_2YGa (Y = Cr, V, and Ni)-based alloys. In a number of previous studies,[41–45] the accuracy of the EMTO-CPA method for the equation of state and elastic properties of metals and disordered alloys has been demonstrated.

For the present application, the EMTO basis sets include s, p, d, and f components, and the scalar-relativistic and soft-core approximations are adopted. The Green function is calculated for 32 complex energy points distributed exponentially on a semicircular contour. As pointed out in Refs. [32,35,36], the EMTO results can be improved by optimizing the overlapping potential spheres. Here, after a careful potential optimization, we set the muffin-tin radii ($R_{\mathrm{mt}}^{\mathrm{Co}}$) and atomic radii ($R_{\mathrm{ws}}^{\mathrm{Co}}$) of the atoms on the Co sublattice being $R_{\mathrm{mt}}^{\mathrm{Co}} = 0.95R_{\mathrm{ws}}$ and $R_{\mathrm{ws}}^{\mathrm{Co}} = 1.10R_{\mathrm{ws}}$, respectively, and keep those of atoms on the other sublattices equal to R_{ws} (Wigner–Seitz radius of the Voronoi polyhedron around each site). In the one-center expansion of the full-charge density, the number of components is truncated at 10. The e/a ratio is calculated with Co-$3d^7 4s^2$, Cr-$3d^5 4s^1$, V-$3d^3 4s^2$, Ni-$3d^8 4s^2$, and Ga-$4s^2 4p^1$. The electronic exchange-correlation potential is described with the generalized gradient approximation by Perdew, Burke, and Ernzerhof.[46] The Brillouin zone is sampled by a $17 \times 17 \times 17$ uniform k-point mesh without smearing technique for both the cubic and tetragonal structures.

The equilibrium lattice parameters (a and c/a) and the bulk modulus (B) of both the $L2_1$ and $D0_{22}$ phases (described clearly in Ref. [12]) are first determined by fitting the calculated total energies (E) versus volume (nine data points) to a Morse function.[47] Here the c/a ratio of the tetragonal structure is defined by means of the equivalent fct (face-centered-tetragonal) unit cell and then, when $c/a = 1$ the tetragonal structure right means the $L2_1$ structure. At the fixed equilibrium volume V, the elastic constants of a single crystal can be derived by straining the lattice and then calculating the second derivative of the total energy ΔE to the strain δ. The lattice deformations and corresponding mathematical formula for the calculation of the elastic constants in both the cubic and tetragonal structures may be found in Ref. [48]. Throughout the present work, in order to get good fitting coefficients, six strains from $\delta = 0$ to 0.05 with intervals of 0.01 are used to calculate the total energies. The corresponding polycrystalline

elastic constants are estimated by means of the Hill average method.[32]

The temperature-dependent magnetism is evaluated with the performance of Uppsala Atomistic Spin Dynamics (UppASD) program.[49–53] Within this method, the itinerant electron system is mapped to an effective classical Heisenberg model,

$$H = -\frac{1}{2}\sum_{i\neq j} J_{ij}\boldsymbol{m}_i \cdot \boldsymbol{m}_j, \tag{1}$$

where J_{ij} are the interatomic exchange interactions, and the indices i and j are 1 and 2, representing the Co and Y atoms. The $\boldsymbol{m}_i$ is the magnetic moment of atom i, its motion is described using the Landau–Lifshitz–Gilbert (LLG) equation[49,50]

$$\begin{aligned}\frac{\partial \boldsymbol{m}_i}{\partial t} &= -\gamma \boldsymbol{m}_i \times [\boldsymbol{B}_i + \boldsymbol{b}_i(t)] - \gamma\frac{\alpha}{m}\boldsymbol{m}_i \\ &\quad \times \{\boldsymbol{m}_i \times [\boldsymbol{B}_i + \boldsymbol{b}_i(t)]\},\end{aligned} \tag{2}$$

where $\boldsymbol{B}_i = -\partial H/\partial \boldsymbol{m}_i$ is the so-called effective field experienced by each atom i, γ is the gyromagnetic ratio, and $\boldsymbol{b}_i(t)$ is a stochastic magnetic field with a Gaussian distribution with respect to temperature T. The magnitude of $\boldsymbol{b}_i(t)$ is related to the damping parameter α, which eventually brings the system into thermal equilibrium. With the solved $\boldsymbol{m}_i$ from Eq. (2), the magnetic moment of the system (M) is then calculated from

$$M(T) = \frac{1}{N}\sqrt{\left(\sum_i m_{x,i}\right)^2 + \left(\sum_i m_{y,i}\right)^2 + \left(\sum_i m_{z,i}\right)^2}. \tag{3}$$

In our calculations, the periodic box size is kept to $10\times 10\times 10$ unit cells. The time-step for solving the above differential Eq. (2) is 10^{-16} s, and the number of the time steps is taken as 10000. The α is set 0.01. The 0 K J_{ij} includes the exchange interactions between the atoms within the tenth nearest neighbors. They are calculated using the magnetic force theorem[54,55] implemented in the EMTO program.[35] The magnetic excitations gradually transform the FM magnetic moment into the PM (described by the disordered local magnetic-moment model,[56] DLM) magnetic moment over a temperature interval of Curie temperature T_C. During this process, with the partially disordered local magnetic-moment (PDLM) model,[57,58] the Co_2YGa system may be described as a $(Co_2^{\uparrow}Y^{\uparrow})_{1-y}(Co_2^{\downarrow}Y^{\downarrow})_y$Ga pseudoalloy. Here, the magnetic disordering degree y is named as the magnetic disordering degree, which is connected with the temperature-dependent normalized magnetic moment ($M/M_0 \approx 1-2y$, with M and M_0 the magnetic moments at any temperature T and 0 K, respectively).

3. Results and discussions

3.1. Equilibrium properties of the austenite

3.1.1. The standard stoichiometric alloys

Table 1 compares the equilibrium properties of the $L2_1$ phase of Co_2YGa (Y = Cr, V, and Ni) alloys with the available experimental and theoretical results.

It is clear that at the FM state, the present a, B, total magnetic moment (μ_{tot}), and magnetic moments on Co (μ_{Co}), Y (μ_Y), and Ga (μ_{Ga}) atoms of the three alloys are in good agreement with their previous theoretical ones.[2,13,62,63,66–68] For Co_2CrGa and Co_2VGa alloys, the a and μ_{tot} values are also in line with their experimental data.[59–61,64,65] Since the atomic radii of Cr, V, and Ni are about 1.85 Å, 1.92 Å, and 1.62 Å, respectively, a of Co_2VGa is the largest whereas that of Co_2NiGa is the smallest. As is expected, a of the two alloys becomes smaller at the PM state (shown in the parentheses). However, in the PM Co_2CrGa alloy, it becomes slightly larger, being consistent with our previous result.[44] It may be attributed that in the alloy, the Co, Cr, and Ga atoms are arranged much more closely together due to their stronger interactions at the ground FM state than the high temperature PM one. B is shown in softening for all the three alloys with the PM ordering.

As listed in Table 1, μ_{Co} turns out to be different in the three FM cubic alloys, and among them the μ_Y values also have big changes. As a result, μ_{tot} of Co_2CrGa alloy is the largest whereas that of Co_2VGa is the smallest. As shown in Fig. 1, the critical temperature, at which M/M_0 gets close to 0 and χ reaches the maximum, thus decreases with Y varying from Cr to Ni and then to V. Their estimated T_C values are about 474 K, 422 K, and 347 K, respectively, also in line with the available experimental data[61,65] in Table 1. Above results ensure the accuracy of the present EMTO and UppASD calculations of these Co_2-based Heusler alloys.

Table 1. Equilibrium lattice parameter (a), bulk modulus (B), total magnetic moment (μ_{tot}), magnetic moments on Co (μ_{Co}), Y (μ_Y), and Ga (μ_{Ga}) atoms, and Curie temperature (T_C) of the FM $L2_1$-Co_2YGa (Y = Cr, V, and Ni) alloys are in comparison with the experimental and theoretical data from Refs. [2,13,59–68]. For comparison, a and B of the three alloys with the PM ordering are also given in the parentheses.

Alloys	Methods	a (Å)	B (GPa)	μ_{tot} (μ_B)	μ_{Co} (μ_B)	μ_Y (μ_B)	μ_{Ga} (μ_B)	T_C (K)
Co_2CrGa	This work	5.7249 (5.7383)	203.5 (177.7)	3.02	0.75	1.57	–0.049	474
	Experiment[59–61]	5.741, 5.805		3.01				495
	Theory[62,63]	5.728	208.8	3.03	0.70	1.72	–0.100	
Co_2VGa	This work	5.7818 (5.7674)	197.3 (183.9)	1.82	0.83	0.18	–0.015	347
	Experiment[61,64,65]	5.7859, 5.769		1.90				352
	Theory[66–68]	5.786	198	2.00	0.92	0.21	–0.008	
Co_2NiGa	This work	5.6959 (5.6882)	181.0 (178.9)	2.56	1.08	0.49	–0.074	422
	Theory[2,13]	5.68	181	2.67				

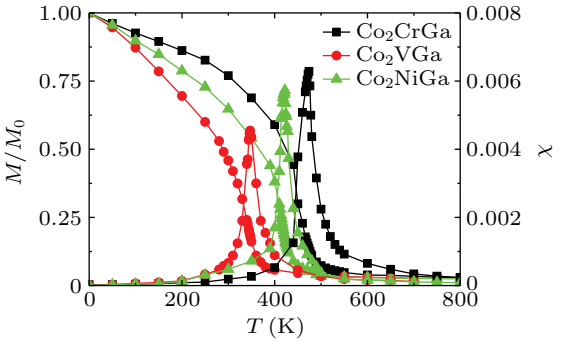


Fig. 1. Temperature dependence of the normalized magnetic moment (M/M_0, with M and M_0 being the magnetic moment at any temperature T and 0 K, respectively) and magnetic susceptibility (χ) of the FM $L2_1$-Co_2YGa (Y = Cr, V, and Ni) alloys.

3.1.2. The off-stoichiometric alloys

For the off-stoichiometric Co_2YGa (Y = Cr, V, and Ni) alloys, we first determine their site preference by comparing the free energies (F) per atom of an alloy with different site occupations at their equilibrium volume. The lower the F is, the more stable the corresponding site configuration is. Here, F is calculated by taking both the electronic total energy E and the chemical mixing entropy into account, expressed as

$$F = E + \frac{1}{4}k_{\mathrm{B}}T\sum_{i=1}^{4}[x_i\ln x_i + (1-x_i)\ln(1-x_i)], \qquad (4)$$

where x_i is the composition at each of the four sublattices, k_{B} is the Boltzmann constant, and $T = 300$ K. We consider the three types of compositions: Co-rich ($Co_{2.1}Y_{0.9}Ga$, $Co_{2.1}YGa_{0.9}$, and $Co_{2.1}Y_{0.95}Ga_{0.95}$), Y-rich ($Co_{1.9}Y_{1.1}Ga$, $Co_2Y_{1.1}Ga_{0.9}$, and $Co_{1.95}Y_{1.1}Ga_{0.95}$), and Ga-rich ($Co_{1.9}YGa_{1.1}$, $Co_2Y_{0.9}Ga_{1.1}$, and $Co_{1.95}Y_{0.95}Ga_{1.1}$) alloys. For each composition, the normal occupancy (the excessive atom evenly occupying all the sites of the deficient atoms) and the abnormal occupancy (the excessive atom occupying solely the site of one of the other two atoms, and then the replaced atoms moving to the sublattice of the left deficient atom) are considered.

In Table 2, the relative electronic total energy (ΔE and $\Delta E'$, for the spin-polarized and nonspin-polarized compositions, respectively, with the same spin-polarized equilibrium lattice constants) as well as free energy (ΔF) of each alloy to that of the alloy with the normal site configuration is shown. For each alloy, the difference between ΔE and ΔF with the same site-occupation configuration is very small at 300 K. Then, around the room temperature, the mixing entropy cannot change the relative stability of the site occupations such that comparing the electronic energy is actually sufficient to determine the stable site occupancy.

For the Co-rich alloys with Y = V and Ni, they always possess the lowest ΔE when the excessive Co atom is in the normal site, i.e., evenly occupies the sites of the deficient atoms, whereas these alloys with Y = Cr are the most stable

Table 2. Relative electronic total energy (ΔE and $\Delta E'$, calculated with and without spin-polarization, in mRy) and free energy (ΔF, in mRy) of the off-stoichiometric $L2_1$-Co_2YGa (Y = Cr, V, and Ni) alloys to those of these alloys with normal site occupancy configuration, at temperature of 300 K. ΔE and $\Delta E'$ are evaluated with the same spin-polarized equilibrium lattice constants. Also presented in the table are the total magnetic moments (μ_{tot}, in μ_{B}) of these FM alloys with different configurations.

Composition	Site occupancy	ΔE			$\Delta E'$			ΔF			μ_{tot}		
		Cr	V	Ni	Cr	V	Ni	Cr	V	Ni	Cr	V	Ni
Co-rich													
$Co_{2.1}Y_{0.9}Ga$	$Co_2(Y_{0.9}Co_{0.1})Ga$	0	0	0	0	0	0	0	0	0	3.08	1.87	2.69
	$Co_2(Y_{0.9}Ga_{0.1})(Ga_{0.9}Co_{0.1})$	1.58	0.46	1.09	0.79	–0.81	0.87	1.43	0.31	0.94	2.36	1.21	2.62
$Co_{2.1}YGa_{0.9}$	$Co_2Y(Ga_{0.9}Co_{0.1})$	0	0	0	0	0	0	0	0	0	2.66	1.45	2.90
	$Co_2(Y_{0.9}Co_{0.1})(Ga_{0.9}Y_{0.1})$	–0.46	1.50	0.62	0.49	0.46	0.30	–0.61	1.35	0.47	3.33	2.03	2.83
$Co_{2.1}Y_{0.95}Ga_{0.95}$	$Co_2(Y_{0.95}Co_{0.05})(Ga_{0.95}Co_{0.05})$	0	0	0	0	0	0	0	0	0	2.83	1.65	2.80
	$Co_2(Y_{0.9}Co_{0.1})(Ga_{0.95}Y_{0.05})$	–2.75	0.67	0.27	0.17	1.10	0.04	–2.81	0.61	0.21	3.21	1.95	2.77
	$Co_2(Y_{0.95}Ga_{0.05})(Ga_{0.9}Co_{0.1})$	–1.82	0.24	0.53	0.05	–0.45	0.15	–1.88	0.18	0.47	2.51	1.33	2.77
Y-rich													
$Co_{1.9}Y_{1.1}Ga$	$(Co_{0.95}Y_{0.05})_2YGa$	0	0	0	0	0	0	0	0	0	2.73	1.37	2.45
	$(Co_{0.95}Y_{0.05})_2Y(Ga_{0.9}Y_{0.1})$	2.85	2.76	3.40	3.58	3.77	3.35	2.70	2.61	3.25	3.31	1.87	2.50
$Co_2Y_{1.1}Ga_{0.9}$	$Co_2Y(Ga_{0.9}Y_{0.1})$	0	0	0	0	0	0	0	0	0	3.30	1.95	2.63
	$(Co_{0.95}Y_{0.05})_2Y(Ga_{0.9}Co_{0.1})$	1.85	2.36	–0.81	–0.44	0.31	–0.17	1.66	2.17	–1.00	2.37	0.98	2.80
$Co_{1.95}Y_{1.1}Ga_{0.95}$	$(Co_{0.975}Y_{0.025})_2Y(Ga_{0.95}Y_{0.05})$	0	0	0	0	0	0	0	0	0	3.02	1.67	2.59
	$(Co_{0.95}Y_{0.05})_2Y(Ga_{0.95}Co_{0.05})$	0.97	1.21	–0.47	–0.18	0.16	–0.06	0.89	1.13	–0.55	2.55	1.19	2.62
	$(Co_{0.975}Ga_{0.025})_2Y(Ga_{0.9}Y_{0.1})$	1.46	1.42	1.70	1.83	1.92	1.60	1.40	1.36	1.64	3.31	1.92	2.57
Ga-rich													
$Co_{1.9}YGa_{1.1}$	$(Co_{0.95}Ga_{0.05})_2YGa$	0	0	0	0	0	0	0	0	0	3.01	1.74	2.32
	$(Co_{0.95}Ga_{0.05})_2(Y_{0.9}Ga_{0.1})Ga$	–2.03	–0.91	–2.03	–3.98	–2.41	–2.59	–2.18	–1.06	–2.18	2.43	1.11	2.08
$Co_2Y_{0.9}Ga_{1.1}$	$Co_2(Y_{0.9}Ga_{0.1})Ga$	0	0	0	0	0	0	0	0	0	2.73	1.61	2.23
	$(Co_{0.95}Ga_{0.05})_2(Y_{0.9}Co_{0.1})Ga$	3.57	4.59	1.96	4.06	4.94	2.59	3.38	4.40	1.77	3.07	1.84	2.48
$Co_{1.95}Y_{0.95}Ga_{1.1}$	$(Co_{0.975}Ga_{0.025})_2(Y_{0.95}Ga_{0.05})Ga$	0	0	0	0	0	0	0	0	0	2.87	1.70	2.32
	$(Co_{0.95}Ga_{0.05})_2(Y_{0.95}Co_{0.05})Ga$	1.77	2.31	0.89	1.97	2.46	1.20	1.69	2.23	0.81	3.03	1.80	2.08
	$(Co_{0.975}Y_{0.025})_2(Y_{0.9}Ga_{0.1})Ga$	–1.06	–0.44	–1.10	–2.06	–1.23	–1.39	–1.12	–0.50	–1.16	2.58	1.39	1.95

when the excessive Co atom occupies the Cr sublattice no matter whether Cr is deficient or not. The Y-rich alloys with $Y =$ Cr and V possess the smallest ΔE when the excessive Y atom takes the normal site as well, whereas when it occupies the Co sublattice these alloys with $Y =$ Ni turn out to be the most stable. The Ga-rich alloys always have the lowest energy when the excessive Ga atom occupies the Y sublattice no matter whether Y is deficient or not. Therefore, it is concluded that in these off-stoichiometric alloys, the excessive Co atom favors the Y sublattice in the $Y =$ Cr alloys, and the excessive Y atom prefers the Co site in the $Y =$ Ni alloys, whereas the excessive Ga atom always tends to take the Y sublattice.

Listed in Table 2 are also $\mu_{\rm tot}$ values of these off-stoichiometric alloys with different site occupations. Examining the local magnetic moments on each sublattices (not shown in the table), we find that both $\mu_{\rm Co}$ and μ_Y change when Co and Y are on the different sublattices. Here, μ_Y corresponding to the Y atom on the Co sublattice is even antiferromagnetic coupling with that to the Y atom on its own site when $Y =$ Cr and V. Therefore, $\mu_{\rm tot}$ of each alloy changes with different site-occupation configurations. Obviously, the site occupancy of these off-stoichiometric Co_2YGa alloys is controlled by the complex interaction between the chemical and magnetic effects. In Table 2, it is seen that ΔE generally differs dramatically from $\Delta E'$, indicating that the magnetic effect on the site occupancy should be very strong. In some groups of Y- and Co-rich alloys, the magnetic effect even alters the stability sequence of the site occupations. Calculated without polarization, instead of being the normal site, the excessive Co atom changes to take the Ga sublattice in the $Y =$ V alloys, and the excessive Y atom changes to occupy the Co site in the $Y =$ Cr alloys. In these off-stoichiometric alloys, the magnetic effect seems to stabilize the normal site-occupation configuration. Contrarily, in the $Y =$ Cr alloys the excessive Co atom is nevertheless found going back to the normal site from nonspin-polarized calculations. The magnetic effect is complicated and composition dependent. It is noted thtat $\mu_{\rm Ga}$ is much small and almost negligible. Calculated with and without spin-polarization, the determined stable site-occupation configurations are the same in each Ga-rich alloy.

With the determined stable site-occupation configuration, we calculate the equilibrium properties of the nine groups of off-stoichiometric alloys: $Co_2Y(Ga_{1-x}Co_x)$ and $Co_2Y(Ga_{1-x}Y_x)$ ($Y =$ Cr, V, and Ni), $Co_2(Y_{1-x}Co_x)Ga$ ($Y =$ Cr and V), and $(Co_{1-0.5x}Ni_{0.5x})_2NiGa$ ($Co_2(Ni_{1+x}Co_{-x})Ga$) alloys ($x = 0.05$, 0.10, 0.15, and 0.20), since in these alloys with increasing x the e/a ratio increases and the MT is then hoped to be promoted. As shown in Table 3, it is found that a of $Co_2Y(Ga_{1-x}Co_x)$ alloys always decreases with increasing x due to the atomic radius of Co (1.67 Å) being much smaller than that of Ga (1.81 Å). Following Vegard' law[69] as well, a of $Co_2(Cr_{1-x}Co_x)Ga$, $Co_2(V_{1-x}Co_x)Ga$, and $Co_2Ni(Ga_{1-x}Ni_x)$ alloys decreases with the increase of x whereas that of $Co_2V(Ga_{1-x}V_x)$ increases with x. Both $Co_2Cr(Ga_{1-x}Cr_x)$ and $(Co_{1-0.5x}Ni_{0.5x})_2NiGa$ alloys are exceptions, where with x increasing from 0 to 0.2, a changes no more than 0.0025 Å, since the atomic radii of Cr (1.85 Å) and Co (1.67 Å) are similar to those of Ga (1.81 Å) and Ni (1.62 Å), respectively. The calculated trends of $B \sim x$ are contrary to those of $a \sim x$ in most groups of these alloys except for $Co_2Cr(Ga_{1-x}Co_x)$, $Co_2(Cr_{1-x}Co_x)Ga$, and $Co_2V(Ga_{1-x}V_x)$, where the trends of $B \sim x$ and $a \sim x$ tend to be the same. In $(Co_{1-0.5x}Ni_{0.5x})_2NiGa$ alloys, due to $\mu_{\rm Ni}$ ($\sim 0.15\mu_{\rm B}$) being much smaller than $\mu_{\rm Co}$ ($\sim 1.07\mu_{\rm B}$), $\mu_{\rm tot}$ decreases with the Ni addition. In all the other alloys, nevertheless, $\mu_{\rm tot}$ always increases with x because there the local magnetic moment of the doped atom is always larger than that of the replaced atom. Even in $Co_2(Cr_{1-x}Co_x)Ga$ alloys, on the same Cr sublattice $\mu_{\rm Co}$ ($\sim 1.75\mu_{\rm B}$) is also larger than $\mu_{\rm Cr}$ ($\sim 1.50\mu_{\rm B}$), although the latter ($\sim 1.57\mu_{\rm B}$) is almost twice the former ($\sim 0.75\mu_{\rm B}$) in the FM $L2_1$-Co_2CrGa alloy.

Table 3. Equilibrium lattice parameter (a, in Å), bulk modulus (B, in GPa), and total magnetic moment ($\mu_{\rm tot}$, in $\mu_{\rm B}$) of nine groups of off-stoichiometric Co_2YGa ($Y =$ Cr, V, and Ni) alloys with the FM $L2_1$ phase: $Co_2Y(Ga_{1-x}Co_x)$ and $Co_2Y(Ga_{1-x}Y_x)$ ($Y =$ Cr, V, and Ni), and $Co_2(Y_{1-\pm x}Co_{\pm x})Ga$ (+ for $Y =$ Cr and V and – for $Y =$ Ni). Four compositions of $x = 0.05$, 0.10, 0.15, and 0.20 are calculated for each group of alloys.

Groups	x	a			B			$\mu_{\rm tot}$		
		Cr	V	Ni	Cr	V	Ni	Cr	V	Ni
$Co_2Y(Ga_{1-x}Co_x)$	0.05	5.7231	5.7762	5.6913	202.8	198.6	182.1	3.17	1.91	2.73
	0.10	5.7210	5.7685	5.6878	202.3	199.6	182.9	3.33	2.00	2.89
	0.15	5.7185	5.7568	5.6842	201.9	200.4	183.2	3.51	2.09	3.04
	0.20	5.7156	5.7420	5.6804	201.7	201.0	183.6	3.67	2.18	3.19
$Co_2Y(Ga_{1-x}Y_x)$	0.05	5.7241	5.7822	5.6928	206.6	197.9	181.3	3.16	1.88	2.67
	0.10	5.7232	5.7827	5.6895	208.4	198.8	181.9	3.30	1.95	2.79
	0.15	5.7224	5.7838	5.6859	208.9	199.7	182.6	3.43	2.01	2.90
	0.20	5.7216	5.7856	5.6824	209.3	200.8	183.7	3.57	2.07	3.00
$Co_2(Y_{1-\pm x}Co_{\pm x})Ga$	0.05	5.7232	5.7752	5.6964	201.9	198.7	179.9	3.06	1.84	2.52
	0.10	5.7215	5.7712	5.6966	200.6	199.8	179.0	3.09	1.87	2.46
	0.15	5.7196	5.7689	5.6968	199.3	200.7	178.4	3.12	1.95	2.39
	0.20	5.7177	5.7677	5.6970	198.1	201.5	177.7	3.15	2.03	2.32

3.2. Martensitic transformation

3.2.1. The stoichiometric alloys with the FM ordering

Figure 2 shows the electronic total energies E of the FM Co_2YGa (Y = Cr, V and Ni) alloys as a function of c/a and r_{ws}. At the ground FM state, E of the three stoichiometric alloys shows two minima: one is at $c/a = 1$, meaning the $L2_1$ parent phase, and another one is around $c/a = 1.25$ for Y = Cr, V and near $c/a = 1.40$ for Y = Ni, corresponding to the tetragonal $D0_{22}$ phase. In comparison, for both Co_2CrGa and Co_2VGa alloys, the $L2_1$ phase is lower than the tetragonal one in energy, meaning that the two stoichiometric alloys can not occur with the MT even at 0 K. Then, the FM cubic phase corresponds to their ground state. For Co_2NiGa alloy, nevertheless, the energy of the obtained $D0_{22}$ structure is lower than that of the $L2_1$ structure. At low temperatures, it can occur with the MT and possess the $D0_{22}$ martensite. The estimated equilibrium V, c/a, B, and μ_{tot} values of the martensitic Co_2NiGa alloy at the FM state are about 11.594 Å^3, 1.3835, 181.1 GPa, and 2.85μ_B, respectively, in good agreement with the previous theoretical results (11.57 Å^3, 1.41, 180 GPa, and 2.92μ_B, respectively).[13]

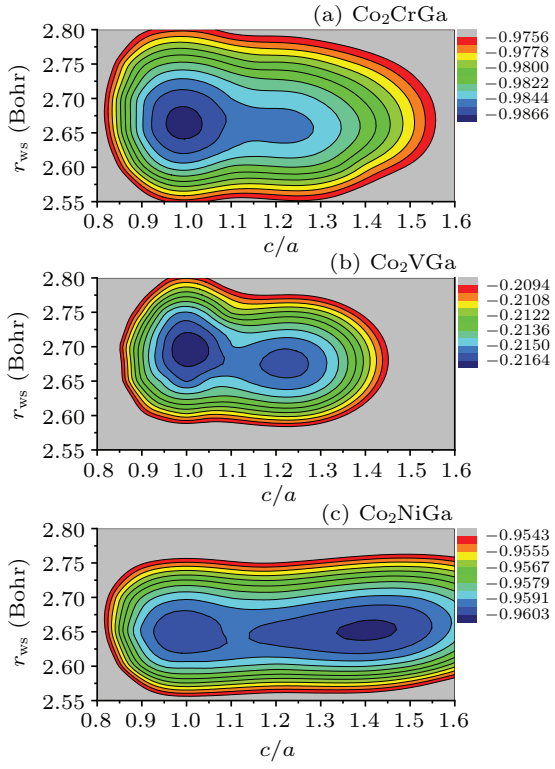


Fig. 2. Electronic total energy (E, in Ry) contours of the FM Co_2YGa (Y = Cr, V, and Ni) alloys as a function of the tetragonal lattice ratio (c/a) and the Wigner–Seitz radius (r_{ws}).

3.2.2. Magnetic disordering effect

In order to investigate the magnetic ordering effect on the MT of Co_2YGa (Y = Cr, V and Ni) alloys, with the fixed equilibrium V at the FM $L2_1$ phase, we calculate their relative electronic total energies ΔE to the $L2_1$ phase change with respect to c/a at the different magnetic disordering degree y values. Their obtained trends of $\Delta E \sim c/a$ change against y are shown in Fig. 3. In each y, we can find two energy minima as well in all the three alloys. The one at $c/a = 1$ means the cubic $L2_1$ phase, whereas another one above $c/a = 1$ corresponds to the tetragonal $D0_{22}$ phase. In Co_2NiGa alloy, with a negative value ΔE of the tetragonal phase ($c/a \sim 1.30$–1.40) decreases with increasing y, indicating that the magnetic disordering further promotes the occurrence of the MT. In Co_2CrGa and Co_2VGa alloys, ΔE of the obtained $D0_{22}$ phase ($c/a \sim 1.20$–1.30) also becomes lower and lower with the increase of y, and when $y = 0.2$ it changes from positive to negative. The critical value of $y = 0.2$ means $M/M_0 = 0.6$. As seen from Fig. 1, in the two alloys it corresponds to T = 390 K and 250 K, respectively. There, before transiting to the PM state, the two stoichiometric alloys thus have already been able to occur with the MT and possess the tetragonal $D0_{22}$ phase. Therefore, contrary to the traditional Ni–Mn–Ga alloys,[70] where during the heating process at low temperatures, the cubic parent phase gets relatively more and more stable, in Co_2CrGa and Co_2VGa alloys the tetragonal $D0_{22}$ martensite gradually changes to be stabilized instead with increasing T due to the magnetic excitations. The magnetic and structural transitions tend to couple each other there, meaning that the metamagnetic MT[5] is also confirmed in the two stoichiometric compositions.

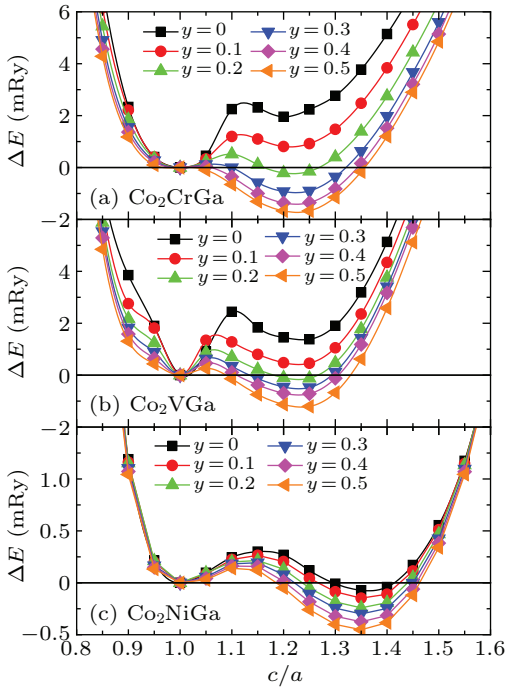


Fig. 3. Relative electronic total energy (ΔE) of Co_2YGa (Y = Cr, V and Ni) alloys to that of their $L2_1$ structure change with respect to the tetragonal lattice distortion (c/a), calculated at the different magnetic disordering degree (y, $0 \le y \le 0.5$).

From Fig. 3, it is also noted that with y increasing from 0 to 0.5, ΔE of the tetragonal martensite decreases about 3.6 mRy and 2.5 mRy in Co_2CrGa and Co_2VGa alloys, respectively, but merely less than 0.5 mRy in Co_2NiGa alloy. In fact,

with the increase of y, μ_{tot} of both the $L2_1$ and $D0_{22}$ phases decreases whereas their E values increase. It is thus obvious that in each $y > 0$, the increase of the energy of the parent phase is higher than that of the tetragonal martensite in the three alloys, and in comparison, the magnetic disordering effect on the relative stability of the $D0_{22}$ martensite is more dominant in Co_2CrGa and Co_2VGa alloys. This result could be attributed to the c/a-dependent μ_{tot} of the three FM (i.e., $y = 0$) alloys. Described in Fig. 4, in the FM Co_2NiGa alloy, the μ_{tot} values corresponding to $c/a = 1$ and 1.40 ($2.6\mu_B$ and $2.8\mu_B$, respectively) are almost comparable and in the alloy, the energy increases of the austenite and martensite in each $y > 0$ are then induced by a similar decrease of their μ_{tot}. However, in the FM Co_2CrGa and Co_2VGa alloys, μ_{tot} of the $L2_1$ phase is much larger than that of the tetragonal phase ($c/a \approx 1.20$–1.25), about $1.5\mu_B$–$1.6\mu_B$. There, in each of $y > 0$ the decrease of μ_{tot} is therefore relatively much more in the austenite. It consequently further accelerates the energy increase of the phase relative to the tetragonal martensite in the two magnetic disordered alloys. In Co_2VGa alloy, μ_{tot} possesses a large value in Fig. 4 only when $c/a = 1$ and 1.05, about $1.82\mu_B$ and $1.48\mu_B$, respectively. For the other c/a values, the Co and V atoms change to be almost non-spin-polarized as well as the Ga atom, and there μ_{tot} is then close to 0. It indicates that the MT of $L2_1$–$D0_{22}$ and the magnetic transition in the alloy may couple each other.

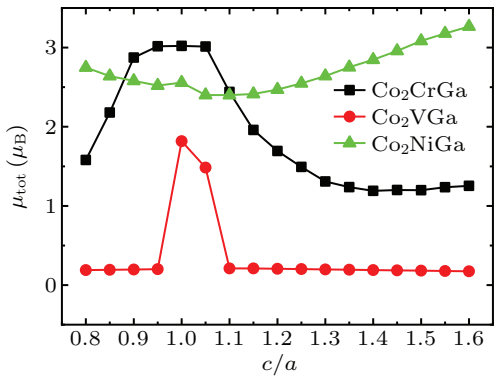


Fig. 4. Total magnetic moments (μ_{tot}) per unit cell of the FM Co_2YGa (Y = Cr, V and Ni) alloys versus the tetragonal lattice distortion (c/a).

At the PM state, Co_2YGa (Y = Cr, V and Ni) alloys are all stabilized by the $D0_{22}$ martensite. The estimated V, c/a, and B values are about 11.686 Å^3, 1.2307, and 194.1 GPa for Co_2CrGa, 11.864 Å^3, 1.2228, and 206.6 GPa for Co_2VGa, and 11.526 Å^3, 1.3509, and 175.6 GPa for Co_2NiGa, respectively. In comparison with the $L2_1$ parent phase, both μ_{Co} and μ_Y of the tetragonal $D0_{22}$ phase in their absolute values greatly decrease in the former two alloys but slightly increase in the last one as well as those of the three FM alloys. As a result, due to the magnetovolume effect:[71] the increase of the local magnetic moment of a system generally corresponding to the expansion of its volume, upon the MT the V values of the three PM alloys change about -1.0%, -1.1%, and 0.2%, respectively, whereas their B values vary about 9.2%, 12.3%, and -1.8%, respectively. For the martensitic Co_2NiGa alloy with the PM ordering, V and c/a are slightly smaller whereas B becomes larger than the corresponding FM alloy.

3.2.3. Alloying effect

We further investigate the alloying effect on the MT in the off-stoichiometric Co_2YGa (Y = Cr, V and Ni) alloys. Since as well as Ni–Mn–Ga, T_M of the most Co_2-based shape memory alloys was also found to increase with e/a,[3,6,18,19] the nine groups of alloys with higher e/a ratio than their stoichiometric compositions shown in Table 3 are considered here. In Fig. 5, their curves of $\Delta E \sim c/a$ changing with respect to x are shown with the energy of the FM $L2_1$ structure ($c/a = 1$) taken as reference at both the FM and PM states. It is found that in each group of Ga-non-deficient $Co_2(Cr_{1-x}Co_x)Ga$, $Co_2(V_{1-x}Co_x)Ga$, and $(Co_{1-0.5x}Ni_{0.5x})_2NiGa$ alloys (Figs. 5(c), 5(f), and 5(i)), the curve of $\Delta E \sim c/a$ changes very small with x increasing from 0 to 0.2 at the two magnetic states. The alloying effect on their MT then seems to be negligible in the studied composition range. In the FM state of $Co_2Y(Ga_{1-x}Co_x)$ and $Co_2Y(Ga_{1-x}Y_x)$ alloys with Y = V (Figs. 5(d) and 5(e)) and Ni (Figs. 5(g) and 5(h)), with increasing x, ΔE of the obtained tetragonal structure above $c/a = 1$ becomes lower and lower. Its value around $c/a = 1.25$ then changes from positive to negative in the two groups of Y = V alloys when x increases up to 0.2 and 0.4, respectively. As well as all the FM Y = Ni alloys, these FM $Co_2V(Ga_{1-x}Co_x)$ and $Co_2V(Ga_{1-x}V_x)$ alloys with $x \geq 0.2$ and $x \geq 0.4$, respectively, then also have the MT behavior at 0 K. With increasing x, the c/a ratio of their $D0_{22}$ structure tends to slightly increase with x (i.e., e/a).

In the FM Ga-deficient alloys with Y = Cr (Figs. 5(a) and 5(b)), the obtained tetragonal structure around $c/a = 1.25$ tends to possess a higher and higher ΔE value with increasing x. This means that, in these alloys, increasing the e/a ratio by replacing the Ga atoms with Co and Cr atoms favors the $L2_1$ parent phase getting more and more stable instead, and then further suppresses the MT. However, it promotes the RMT from $D0_{22}$ to $L2_1$ there at low temperatures. Correspondingly, T_M for their RMT then tends to decrease with increasing x (e/a) since the energy barrier between the two phases becomes lager and larger with Co and Cr doping. The established contrary trends of $T_M \sim x$ for the MT at the PM state and the RMT at the FM state are in good agreement with those measured in the $Co_2Cr(GaSi)$ shape memory alloys.[3]

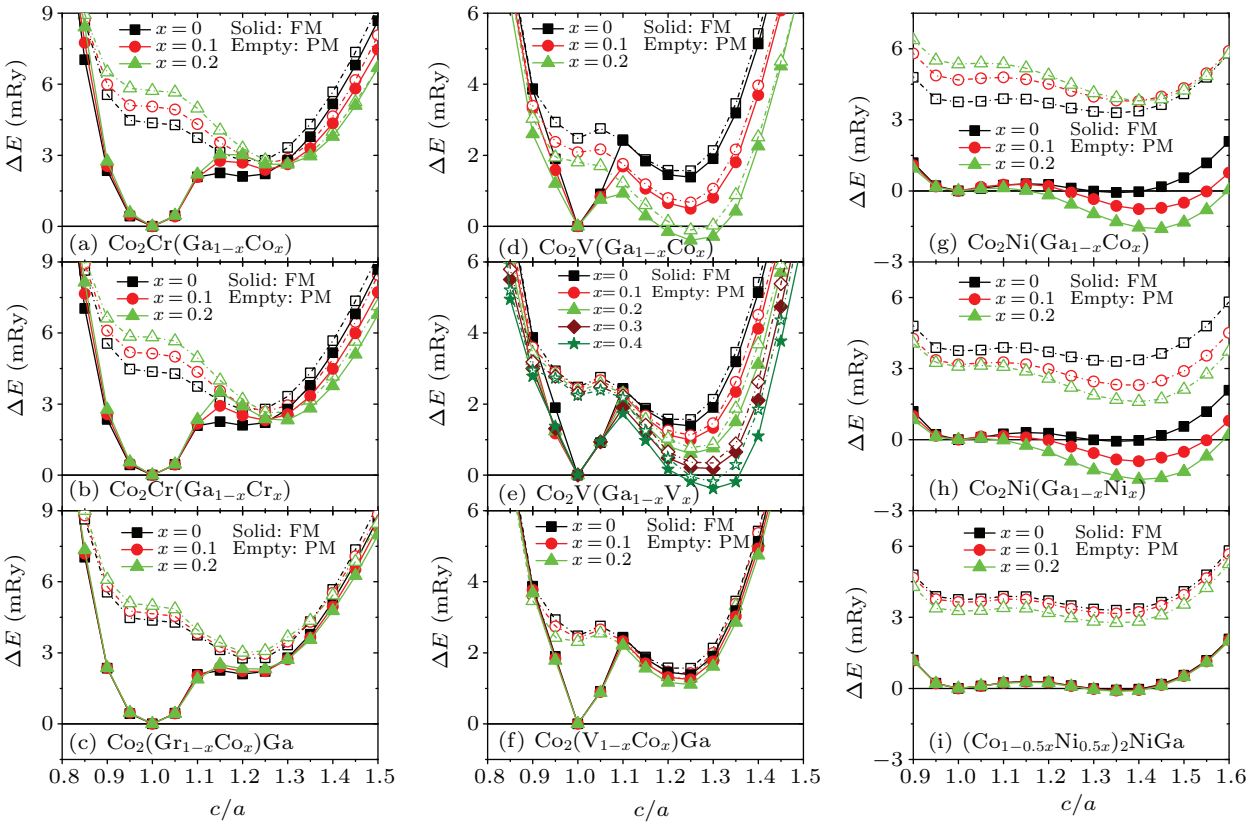


Fig. 5. Relative electronic total energies (ΔE) of the FM and PM $Co_2Y(Ga_{1-x}Co_x)$ and $Co_2Y(Ga_{1-x}Y_x)$ (Y = Cr, V, and Ni), $Co_2(Y_{1-x}Co_x)Ga$ (Y = Cr and V), and $(Co_{1-0.5x}Ni_{0.5x})_2NiGa$ alloys versus the tetragonal lattice distortion (c/a). Here, the electronic energy of the FM $L2_1$ structure ($c/a = 1$) is taken as reference for each alloy. The range of concentration x is $0 \le x \le 0.4$ for $Co_2V(Ga_{1-x}V_x)$ and $0 \le x \le 0.2$ for the other groups of alloys.

At the PM state, ΔE of each alloy corresponding to the $D0_{22}$ structure is always lower than that to the $L2_1$ one in Fig. 5, and then all these PM off-stoichiometric alloys can occur with the MT as well. In the Ga-deficient $Co_2Y(Ga_{1-x}Co_x)$ and $Co_2Y(Ga_{1-x}Y_x)$ alloys, with increasing x (i.e., e/a), the c/a ratio of the tetragonal martensite slightly increases, whereas ΔE corresponding to the structure gradually becomes lower and lower than that to the $L2_1$ structure. Then, the $D0_{22}$ phase becomes more and more stable than the $L2_1$ phase with Co and Y doping. This indicates that in these PM alloys, the MT is promoted with the increase of e/a, corresponding to the increase of their T_M with e/a. It is also noted that in all these Y = Cr and V alloys, ΔE of the $D0_{22}$ structure corresponding to the PM state is always not much higher than that to the FM one, and in some compositions they are even similar. It indicates the low magnetization and magnetic excitation energy of their tetragonal phase. The MT of $L2_1$–$D0_{22}$ therefore should tend to couple with the magnetic or metamagnetic transition in these Y = Cr and V alloys.

3.3. Elastic properties

3.3.1. The standard stoichiometric alloys

Table 4 lists the calculated static elastic constants of the stoichiometric Co_2YGa (Y = Cr, V and Ni) alloys with the austenitic and martensitic phases, in comparison with the previous theoretical results.[2,45,72] It is shown that in the FM $L2_1$ phase of the three alloys, the present C_{11} is slightly smaller but C_{12} becomes slightly larger than our previous results calculated with the normal settings of R_{mt} and R_{ws} (i.e., R_{mt} and R_{ws} on all the sublattices are equal to R_{ws}).[45] As a result, their estimated C' values as well as C_{44} are smaller than those corresponding to the previous EMTO calculations.[45] However, it is clear that with the optimized R_{mt}^{Co} and R_{ws}^{Co} ($R_{mt}^{Co} = 0.95R_{ws}$ and $R_{ws}^{Co} = 1.10R_{ws}$), the evaluated shear elastic constant C' and C_{44} are closer to those resulted from the first-principles full potential calculations shown in Table 4,[2,72] confirming again the accuracy of our present EMTO calculations.

The magnetic excitations gradually transform the system from the FM state to the PM one. Correspondingly, the elastic constants of Co_2YGa (Y = Cr, V, and Ni) alloys can be assumed to change against the magnetic disordering degree y increasing from 0 to 0.5. Here, with the equilibrium volume at the FM state ($y = 0$), C', C_{44} and the elastic anisotropy (A) of the three $L2_1$ alloys are then especially calculated at the different y values. As shown in Fig. 6, with increasing y, both C' and C_{44} of the Y = Cr and V alloys decrease whereas for the Y = Ni alloy, C' decreases and C_{44} increases with y. The evaluated A values of the three alloys all gradually increase with the increase of y. This result indicates that in the three alloys, the magnetic disordering tends to soften the tetragonal shear elastic constant C' and then increase their elastic anisotropy

A. Described in Table 4, when the FM state transiting to the PM one, C' decreases to 62.1% and A increases to 1.6 times for Co_2NiGa, for Co_2CrGa C' decreases to 7.7% and A increases to 10.7 times, and for Co_2VGa C' even becomes negative. Thus, the magnetic disordering decreases the mechanical stability of the $L2_1$ parent phase, which nevertheless favors the tetragonal lattice deformations and then promotes the MT in the three stoichiometric alloys.

Table 4. Single crystal elastic constants (in GPa), tetragonal shear elastic constant ($C' = (C_{11} - C_{12})/2$ and $C_s = C_{11} + C_{12} + 2C_{33} - 4C_{13}$, for the cubic and tetragonal structures, respectively, in GPa), shear modulus (G, in GPa), Young modulus (E, in GPa), Debye temperature (Θ, in K), elastic anisotropy (A), and the ratio of the shear and bulk modulus (G/B) of the FM and PM Co_2YGa (Y = Cr, V, and Ni) alloys with the $L2_1$ and $D0_{22}$ phases, in comparison with those of theoretical ones taken from Refs. [2,45,72].

Phases	Alloys	Methods	C_{11}	C_{12}	C_{13}	C_{33}	C_{44}	C_{66}	C'/C_s	G	E	Θ	A	G/B
FM-$L2_1$	Co_2CrGa	**This work**	**238.3**	**186.1**			**137.0**		**26.1**	**68.6**	**184.9**	**418.9**	**5.25**	**0.34**
		Previous work[45]	240.3	185.1			137.3		27.6	70.4	189.3	424.2	4.97	0.35
		Ref. [72]	233.0	182.8			136.8		25.1	67.3			5.45	0.34
	Co_2VGa	**This work**	**265.2**	**163.4**			**130.9**		**50.9**	**89.2**	**232.5**	**478.3**	**2.57**	**0.45**
		Previous work[45]	277.7	157.1			143.1		58.3	100.8	258.4	507.1	2.46	0.51
		Ref. [72]	266.5	162.1			126.8		52.2	88.5			2.43	0.45
	Co_2NiGa	**This work**	**188.7**	**177.1**			**127.1**		**5.8**	**32.7**	**92.4**	**287.0**	**21.91**	**0.18**
		Previous work[45]	195.4	173.8			137.7		10.8	45.9	126.9	338.6	12.75	0.25
		Ref. [2]	197	187			120		5				24	
PM-$L2_1$	Co_2CrGa	This work	180.4	176.4			121.8		2.0	19.0	55.0	223.7	56.39	0.11
	Co_2VGa	This work	180.1	185.8			106.8		–2.9					
	Co_2NiGa	This work	225.7	136.5			129.1		3.6	26.1	74.6	257.0	35.92	0.15
FM-$D0_{22}$	Co_2NiGa	This work	225.5	148.4	169.4	204.5	128.0	94.6	105.1	61.0	164.6	389.0		0.34
PM-$D0_{22}$	Co_2CrGa	This work	267.9	146.5	167.9	246.5	134.6	147.3	235.9	90.2	234.2	476.9		0.46
	Co_2VGa	This work	260.5	174.8	184.5	250.8	107.4	168.9	198.9	76.8	204.9	444.2		0.37
	Co_2NiGa	This work	225.7	136.5	164.5	197.7	146.0	111.9	99.6	66.5	177.0	404.7		0.38

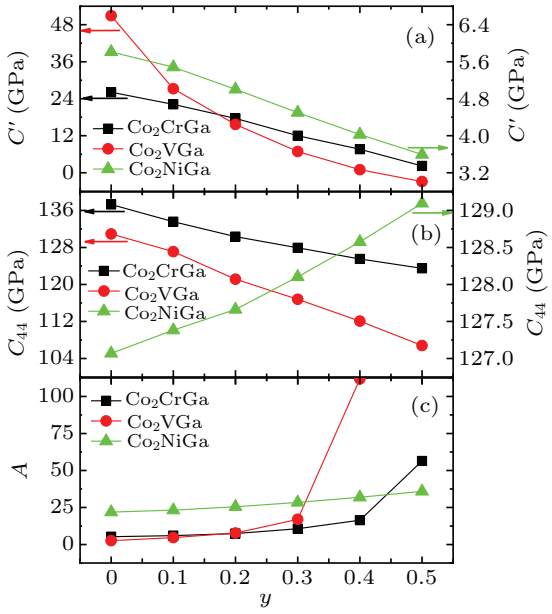


Fig. 6. Shear elastic constants (C' and C_{44}) and elastic anisotropy (A) of $L2_1$-Co_2YGa (Y = Cr, V, and Ni) alloys versus the magnetic disordering degree (y) increasing from 0 to 0.5.

The stability criteria for tetragonal crystals are $C_{11} > |C_{12}|$, $C_{33} > 0$, $C_{44} > 0$, $C_{66} > 0$, $C_{11} + C_{33} - 2C_{13} > 0$, and $C_s (= C_{11} + C_{12} + 2C_{33} - 4C_{13}) > 0$. From our calculations shown in Table 4, the elastic constants of the tetragonal alloys all satisfy the above conditions. It indicates that at 0 K, the tetragonal martensite is energetically and mechanically stabilized in the PM Co_2CrGa and Co_2VGa alloys, as well as in both the FM and PM Co_2NiGa alloys. For the FM $D0_{22}$-Co_2NiGa alloy, the present elastic constants seem to be comparable with those theoretical ones of the FM $L1_0$-CoNiGa alloy.[16]

The plastic property of a material has been related to the ratio of the shear and bulk modulus (G/B). A high value of G/B (greater than ~ 0.57) generally means the inherent crystalline brittleness (ICB) of a bulk material. From Table 4, we find that the G/B values of these stoichiometric alloys are all below this critical value and hence their ICB is low. In comparison with the FM ordering, the PM ordering also tends to decrease the G/B ratio of these cubic alloys. However, the MT seems to increase the ICB of these alloys. In both the FM and PM Co_2NiGa and PM Co_2CrGa alloys, the G/B ratio of the martensite is always larger than that of the austenite.

3.3.2. The off-stoichiometric alloys

Figure 7 shows C', C_{44}, and A values of the FM and PM $L2_1$ phase of the studied nine groups of off-stoichiometric Co_2YGa (Y = Cr, V and Ni) alloys change with respect to the composition x. For all the Ga-deficient $Co_2Y(Ga_{1-x}Co_x)$ and $Co_2Y(Ga_{1-x}Y_x)$ alloys, both C' and C_{44} decrease with increasing x (i.e., e/a) at the PM state, whereas their A values of these Y = V (Figs. 7(d), 7(e), and 7(f)) and Ni (Figs. 7(g), 7(h), and 7(i)) alloys increase with x. For the Y = Cr (Figs. 7(a), 7(b), and 7(c)) alloys with the PM ordering, A has not been shown in Fig. 7(c) since their C' values are negative. The x-dependent C' as well as A of these PM Ga-deficient alloys indicates that their $L2_1$ parent phase gets mechanically more and more unstable with the increase of e/a ratio, which nevertheless favors

the tetragonal lattice deformations. At the FM state, both C' and C_{44} decrease with the increase of x in these Ga-deficient Y = V alloys whereas in the corresponding Y = Ni alloys, C' decreases but C_{44} increases with x. As a result, A of all these Y = V and Ni alloys increases with x as well. Similar to their corresponding PM alloys, with the increase of e/a ratio, C' softens whereas A enhances, promoting the MT from $L2_1$ to $D0_{22}$. Correspondingly, as shown in Fig. 5, with increasing x the tetragonal phase of all these PM Ga-deficient alloys and the FM ones without Y = Cr gets relatively lower and lower in energy in comparison with the $L2_1$ parent phase.

For the FM $L2_1$ phase of $Co_2Cr(Ga_{1-x}Co_x)$ and $Co_2Cr(Ga_{1-x}Cr_x)$ alloys, with increasing x both C' and C_{44} increase whereas A decreases. In these alloys, the $L2_1$ parent phase gets mechanically more and more stable instead with the increase of e/a ratio, contrary to their corresponding Y = V and Ni alloys. Correspondingly, as shown in Figs. 5(a) and 5(b), respectively, upon tetragonal lattice distortions, the cubic $L2_1$ phase of the two groups of Ga-deficient Y = Cr alloys becomes lower and lower in energy with increasing x in comparison with the obtained tetragonal phase, promoting the RMT from $D0_{22}$ to $L2_1$.

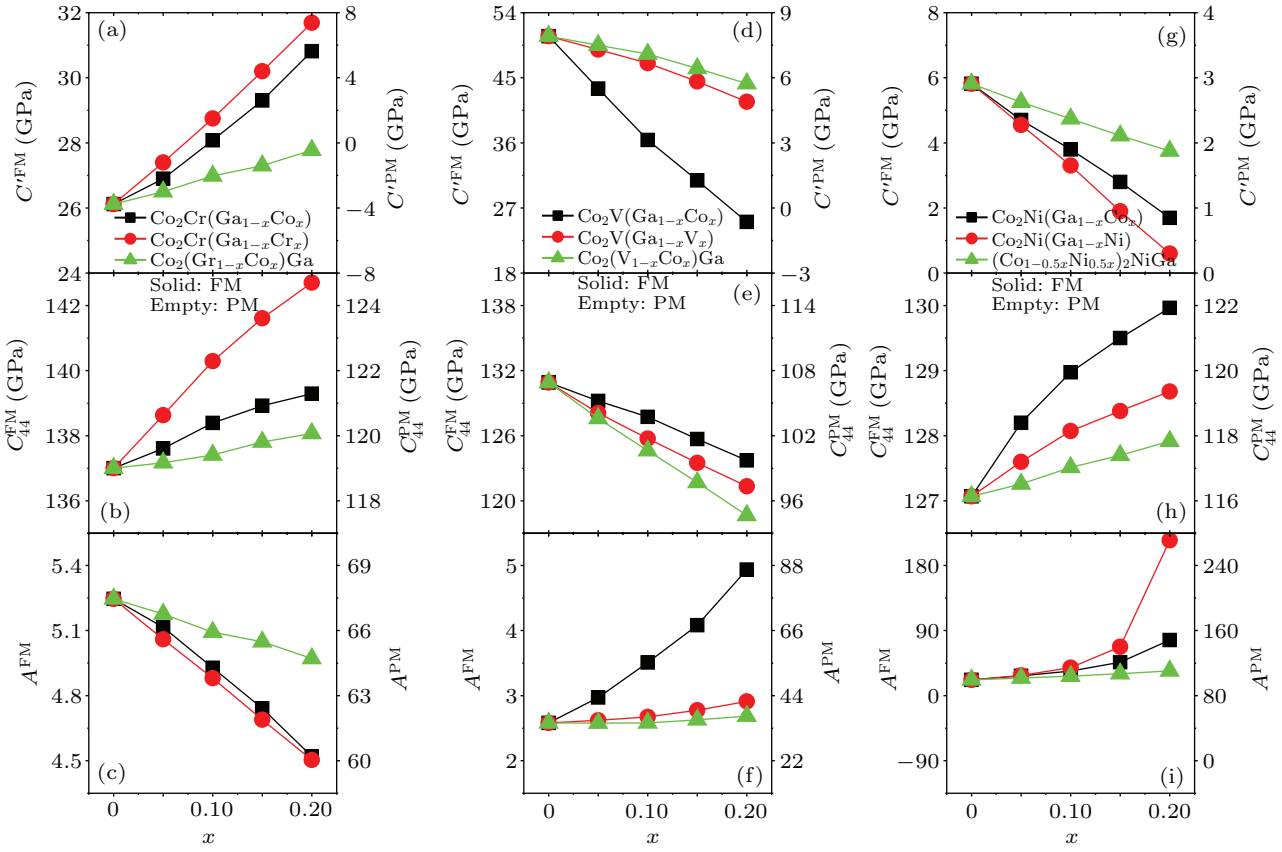


Fig. 7. Shear elastic constants (C' and C_{44}) and elastic anisotropy (A) of the FM and PM $L2_1$ phase of $Co_2Y(Ga_{1-x}Co_x)$ and $Co_2Y(Ga_{1-x}Y_x)$ (Y = Cr, V and Ni), $Co_2(Y_{1-x}Co_x)Ga$ (Y = Cr and V), and $(Co_{1-0.5x}Ni_{0.5x})_2NiGa$ alloys versus the composition x ($0 \le x \le 0.2$).

For both the FM and PM $L2_1$ phases of $Co_2(Y_{1-x}Co_x)Ga$ (Y = Cr and V) and $(Co_{1-0.5x}Ni_{0.5x})_2NiGa$ alloys, the evaluated trends of $C' \sim x$, $C_{44} \sim x$, and $A \sim x$ are in line with those of their corresponding Ga-deficient alloys. In comparison, nevertheless, with x increasing from 0 to 0.2, the variations of C' and A are relatively smaller in each group of these Ga-non-deficient alloys. Then, the alloying effect on their elastic stabilities should be not as significant as it on those of the corresponding Ga-deficient alloys. Similarly, their curves of $\Delta E \sim c/a$ at both the magnetic states also have not a big change with x increasing from 0 to 0.2 in Figs. 5(c), 5(f), and 5(i). Therefore, in these studied Ga-deficient $Co_2Y(Ga_{1-x}Co_x)$ and $Co_2Y(Ga_{1-x}Y_x)$ alloys, the composition dependence of the MT is closely related with their composition-dependent C' and A values: the increase of the e/a ratio generally corresponds to the decrease of C' but the increase of A, which promotes the occurrence of the MT but suppresses the RMT behavior.

3.4. Electronic structure

To understand the atomistic origin of the phase stability of these studied Co_2YGa-based Heusler alloys, we compare the total density of states (DOS) of their stoichiometric compositions with both the FM and PM $L2_1$ and $D0_{22}$ phases. As shown in Figs. 8(a) and 8(e), respectively, in the FM $L2_1$ phase of Co_2CrGa and Co_2VGa alloys, around the Fermi level there is a big peak in the majority (spin-up) DOS, while there is a deep band gap in the minority (spin-down) DOS, indicating that the two alloys exhibit a nearly half-metallic behav-

ior in the FM cubic phase. As seen from the local DOS of Co (Figs. 8(b) and (f)), Cr and V (Figs. 8(c) and 8(g)), and Ga (Figs. 8(d) and 8(h)) atoms, it is clear that the big peak is contributed mainly by the degenerated Co d and Cr d (V d) electronic states, whereas the deep band gap originates mainly from the overlapping of the orbits between Co d and Ga p as well as Cr d (V d) and Ga p, i.e., the strong covalent hybridization between them around the Fermi level.

Upon tetragonal distortions, the degenerated Co d and Cr d (V d) states dominating the big peak around the Fermi level split and there, these states may shift to lower or higher energy levels. Then, in the FM $D0_{22}$ phase the big peak becomes smaller in Co_2CrGa and it even disappears in Co_2VGa. The redistribution of the majority DOS has nevertheless no great influence on the stability of the system. However, in the minority DOS, the deep band gap around the Fermi level becomes shallower in the two FM tetragonal alloys, since there the Co d and Cr d (V d) states increase upon tetragonal distortions. It indicates that in the FM $D0_{22}$ phase, the covalent banding between Co and Ga as well as Cr (V) and Ga weakens, and the stability of the system then beomces worse. The calculated tetragonal shear elastic constant C' of the FM $L2_1$ phase of the two alloys are thus with very large values. With Co and Cr (V) substituting for Ga, this electronic structure mechanism should beomce more and more dominant, further suppressing the tetragonal lattice deformations. In the Ga-deficient $Co_2Cr(Ga_{1-x}Co_x)$ and $Co_2Cr(Ga_{1-x}Cr_x)$ alloys with the FM ordering (Figs. 5(a) and 5(b), respectively), the calculated relative electronic energy ΔE of the tetragonal $D0_{22}$ phase is thus higher and higher with increasing x, whereas C' of the $L2_1$ phase increases but A decreases with x (Figs. 7(a) and 7(c), respectively). In all these $Y = $ Cr alloys, the FM $L2_1$ phase is the ground state.

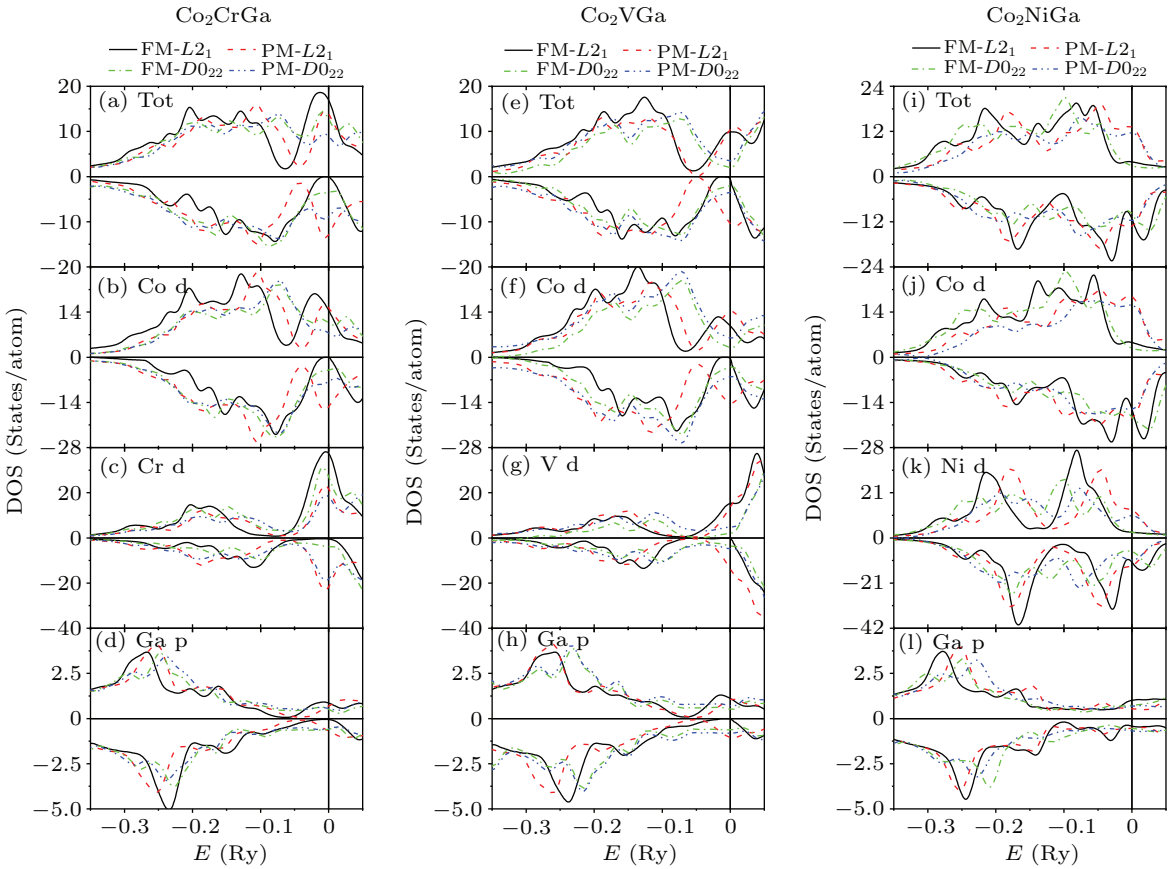


Fig. 8. Total electronic density of states (DOS) [(a), (e), and (i)] and local DOS corresponding to Co [(b), (f), and (j)], Y [(c), (g), and (k)], and Ga [(d), (h), and (l)] of Co_2YGa (Y = Cr, V and Ni) alloys with both the FM and PM $L2_1$ and $D0_{22}$ phases. The vertical lines indicate the Fermi level.

Unlike Co_2CrGa alloy where the valley of the band gap is almost right at the Fermi level, in the FM $L2_1$ phase of Co_2VGa alloy, the right sides of the band gap for Co d and Vd and then that for the total DOS are very close to the Fermi level. Consequently, upon tetragonal distortions, there some of the Co d and V d states (dominated by the former) shift near below the Fermi level. Then, the band gap in the total DOS of the alloy becomes shallower but wider at the same time in the FM $D0_{22}$ phase. Replacing Ga with Co and V in Co_2VGa alloy, the widening of the band gap should also become more and more significant as well as its getting shallow upon tetragonal distortions. However, contrary to the latter, the former indicates the covalent banding between Co and Ga as well as Cr and Ga getting stronger and stronger, and then ΔE of the $D0_{22}$ phase becomes lower and lower with Co and V doping. It favors C' of the $L2_1$ phase decreasing but A increasing with

x in $Co_2V(Ga_{1-x}Co_x)$ and $Co_2V(Ga_{1-x}V_x)$ alloys. Obviously, since in comparison with the corresponding $Y = Cr$ alloys, the contrary trends of $\Delta E \sim x$ (Figs. 5(d) and 5(e)), $C' \sim x$ (Fig. 7(d)), and $A \sim x$ (Fig. 7(f)) are estimated in these FM $Y = V$ alloys, upon tetragonal distortions the widening of the band gap is confirmed to have more and more dominant role on the phase stability than its getting shallow with Co and V doping in these alloys. Moreover, in comparison, the Co-doping should more favor this electronic structure mechanism, since upon tetragonal distortions the DOS change of Co d seems to be slightly larger than that of V d around the band gap in Co_2VGa alloy. In each x, C' is therefore relatively lower in the Co-doped alloys in Fig. 7(d) and shown in Fig. 5(d), when x goes up to 0.2, $Co_2V(Ga_{1-x}Co_x)$ alloys turn out to possess the MT behavior, whereas $Co_2V(Ga_{1-x}V_x)$ alloys can occur with the MT until $x \geq 0.4$ in Fig. 5(e). Only in the two groups of Ga-deficient $Y = V$ alloys with $x < 0.2$ and $x < 0.4$, respectively, the FM $L2_1$ phase corresponds the ground state.

As shown in Fig. 8(i), in the FM $L2_1$-Co_2NiGa alloy, there are both majority and minority DOS located around the Fermi level, showing the metallic property of the alloy. Moreover, around the Fermi level in the minority DOS of the alloy, there is a pseudogap contributed by the overlapping of the orbits between Co d and Ga p as well as Ni d and Ga p. Upon tetragonal distortions, the pseudogap corresponding to Ni d becomes deeper and wider, and that for Co d becomes slightly shallower but wider. As a result, the pseudogap in the total DOS becomes wider in the FM $D0_{22}$ phase, indicating the stronger covalent banding between Co and Ga as well as Ni and Ga, and then the more stability of the system. Thus, in Co_2NiGa alloy the FM tetragonal phase corresponds to the ground state. This phase should further become relatively more and more stable with Co and Ni substituting for Ga and in comparison, the Ni-doping has a greater influence on its relative stability. Similarly, in each x, the evaluated C' value of the Ni-doped alloys (Fig. 5(g)) is also smaller than that of the Co-doped alloys (Fig. 5(h)).

At the PM state, there is a big peak just right at the Fermi level in the $L2_1$ phase of all the three stoichiometric alloys, dominated by the Co d and Y d states. Similar to Ni–Mn–Ga alloys, this big peak results in the instability of the cubic parent phase due to the Jahn–Teller effect.[30,31] Upon tetragonal distortions, these Co d and Y d states around the Fermi level split, and there the peak in the total DOS then beomces smaller. Since the decrease of the states just right at the Fermi level lowers the energy of the system, the tetragonal $D0_{22}$ phase is thus stabilized in all the three PM alloys. With Co and Y substituting for Ga, this electronic structure mechanism becomes more and more effective. Then, in all the Ga-deficient alloys with the PM ordering, with Co and Y doping, C' of the $L2_1$ phase decreases whereas A increases and upon tetragonal distortions, the $D0_{22}$ phase becomes relatively more and more stable.

4. Summary

Using the first-principles EMTO-CPA method, we have systematically investigated the alloying and magnetic disordering effects on the site occupation, equilibrium properties, elastic property, and phase stability of $L2_1$- and $D0_{22}$-Co_2YGa (Y = Cr, V, and Ni) Heusler alloys. The main results are summarized as follows:

(1) At the ground FM state, both Co_2CrGa and Co_2VGa alloys possess the $L2_1$ structure whereas Co_2NiGa alloy is stabilized by the $D0_{22}$ martensite. At the PM state, all the three stoichiometric alloys can show the martensitic transformation (MT) behavior and then have the tetragonal structure. Their evaluated crystal structure and lattice parameters, μ_{tot} and T_C values, and elastic constants for both the austenite and martensite are in good agreement with the experimental and theoretical results.

(2) For the three stoichiometric alloys, with increasing the magnetic disordering degree y, their C' of the $L2_1$ phase decreases but A increases, and upon tetragonal distortions the cubic phase becomes relatively more and more unstable. For $y \geq 0.2$, Co_2CrGa and Co_2VGa alloys thus can show the MT from $L2_1$ to $D0_{22}$ as well. In comparison with Co_2NiGa, in the two alloys the magnetic disordering effect on the relative stability of the $D0_{22}$ phase is more dominant since at their FM state, μ_{tot} of the $L2_1$ phase is much larger than that of the $D0_{22}$ phase, which further accelerates the energy increase of the former relative to the latter in each $y > 0$.

(3) In off-stoichiometric alloys, the site preference is controlled by both the alloying and magnetic effects. From spin-polarized calculations, the excessive Ga atom always tends to take the Y sublattice, whereas the excessive Co atom favors the Y site when Y = Cr, and the excessive Y atom prefers the Co site when Y = Ni. Calculated without spin-polarization, instead of being the normal site, the excessive Y atom changes to take the Co site when Y = Cr and the excessive Co atom changes to occupy the Ga site when Y = V, whereas in the Y = Cr alloys, the excessive Co atom goes back to the normal site.

(4) In the Ga-deficient $Co_2Y(Ga_{1-x}Co_x)$ and $Co_2Y(Ga_{1-x}Y_x)$ alloys with the PM ordering, with increasing x (i.e, e/a), C' of the $L2_1$ phase decreases but A increases, whereas the relative electronic energy ΔE of the $D0_{22}$ phase becomes lower and lower, which corresponds to T_M increasing with e/a. The same trends of $C' \sim x$, $A \sim x$, $\Delta E \sim x$ are also found in these FM Y = V and Ni alloys, resulting that the two groups of Y = V alloys with $x \geq 0.2$ and 0.4, respectively, can occur with the MT also at the FM state. However, in the corresponding FM Y = Cr alloys, their contrary trends

are established, indicating that with the increase of e/a, the RMT from $D0_{22}$ to $L2_1$ is promoted and then T_M for the RMT should decrease.

(5) The x-dependent MT in $Co_2Y(Ga_{1-x}Co_x)$ and $Co_2Y(Ga_{1-x}Y_x)$ alloys is finally well explained by means of the Jahn–Teller effect at the PM state. At the FM state, it may originate from the competition between the austenite and martensite about their strength of the covalent banding between Co and Ga as well as Y and Ga. With increasing x, it becomes relatively stronger and stronger in the austenite for the $Y =$ Cr alloys but in the martensite for the $Y =$ V and Ni alloys, which consequently promotes the RMT for the former alloys but the MT for the latter ones.

Acknowledgements

This work was supported by the National Natural Science Foundation of China (Grant Nos. 12174269, 11674233 and 51301176), the China Postdoctoral Science Foundation (Grant Nos. 2013M530133 and 2014T70264), and the Natural Science Foundation of Liaoning Province, China (Grant Nos. 2019-MS-287 and L201602672).

References

[1] Wuttig M, Li J and Craciunescu C 2001 *Scr. Mater.* **44** 2393
[2] Arróyave R, Junkaew A, Chivukula A, Bajaj S, Yao C Y and Garay A 2010 *Acta Mater.* **58** 5220
[3] Xu X, Nagasako M, Kataoka M, Umetsu R Y, Omori T, Kanomata T and Kainuma R 2015 *Phys. Rev. B* **91** 104434
[4] Odaira T, Xu X, Miyake A, Omori T, Tokunaga M and Kainuma R 2018 *Scr. Mater.* **153** 35
[5] Liu C Q, Li Z, Zhang Y L, Huang Y S, Ye M F, Sun X D, Zhang G J, Cao Y M, Xu K and Jing C 2018 *Appl. Phys. Lett.* **112** 211903
[6] Xu X, Nagashima A, Nagasako M, Omori T, Kanomata T and Kainuma R 2017 *Appl. Phys. Lett.* **110** 121906
[7] Obaidallah A, Algethami A, Zhang Q Q, Tan J G, Wang X T, Liu Z H and Ma X Q 2020 *J. Magn. Magn. Mater.* **498** 166252
[8] Huang Y, Jing C, Li J, Zhang Y, Zhang G and Qin N 2020 *J. Magn. Magn. Mater.* **513** 167059
[9] Li C M, Zhou J P, Yang S J and Zhang Y 2021 *Comput. Mater. Sci.* **196** 110527
[10] Jiang H X, Xu X, Omori T, Nagasako M, Ruan J J, Yang S Y, Wang C P, Liu X J and Kainuma R 2016 *Mater. Sci. Eng. A* **676** 191
[11] Jiang H X, Wang C P, Xu W W, Xu X, Yang S Y, Kainuma R and Liu X J 2017 *Mater. Des.* **116** 300
[12] Xu X, Omori T, Nagasako M, Okubo A, Umetsu R Y, Kanomata T, Ishida K and Kainuma R 2013 *Appl. Phys. Lett.* **103** 164104
[13] Siewert M, Gruner M E, Dannenberg A, Hucht A, Shapiro S M, Xu G, Schlagel D L, Lograsso T A and Entel P 2010 *Phys. Rev. B* **82** 064420
[14] Singh N, Dogan E, Karaman I and Arróyave R 2011 *Phys. Rev. B* **84** 184201
[15] Dogan E, Karaman I, Singh N, Chivukula A, Thawabi H S and Arróyave R 2012 *Acta Mater.* **60** 3545
[16] Talapatra A, Arróyave R, Entel P, Valencia-Jaime I and Romero A H 2015 *Phys. Rev. B* **92** 054107
[17] Sahay S and Goswami B 2009 *Solid State Phenom.* **150** 197
[18] Craciunescu C, Kishi Y, Lograsso T A and Wutting M 2002 *Scr. Mater.* **47** 285
[19] Li Y, Xin Y, Chai L, Ma Y and Xu H 2010 *Acta Mater.* **58** 3655
[20] Xu X, Omori T, Nagasako M, Kanomata T and Kainuma R 2015 *Appl. Phys. Lett.* **107** 181904
[21] Xin Y, Li Y, Jiang C B and Xu H B 2005 *Mater. Sci. Forum* **475–479** 1991
[22] Seguí C, Pons J and Cesari E 2007 *Acta Mater.* **55** 1649
[23] Hu Q M, Luo H B, Li C M, Vitos L and Yang R 2012 *Sci. China Tech. Sci.* **55** 295
[24] Chen J, Li Y, Shang J X and Xu H B 2006 *Appl. Phys. Lett.* **89** 231921
[25] Bungaro C, Rabe K M and Corso A Dal 2003 *Phys. Rev. B* **68** 134104
[26] Stipcich M, Mañosa L, Planes A, Morin M, Zarestky J, Lograsso T and Stassis C 2004 *Phys. Rev. B* **70** 054115
[27] Banik S, Ranjan R, Chakrabarti A, Bhardwaj S, Lalla N P, Awasthi A M, Sathe V, Phase D M, Mukhopadhyay P K, Pandey D and Barman S R 2007 *Phys. Rev. B* **75** 104107
[28] Lanska N, Söderberg O, Sozinov A, Ge Y, Ullakko K and Lindroos V K 2004 *J. Appl. Phys.* **95** 8074
[29] Li C M, Luo H B, Hu Q M, Yang R, Johansson B and Vitos L 2012 *Phys. Rev. B* **86** 214205
[30] Opeil C P, Mihaila B, Schulze R K, Mañosa L, Planes A, Hults W L, Fisher R A, Riseborough P S, Littlewood P B, Smith J L and Lashley J C 2008 *Phys. Rev. Lett.* **100** 165703
[31] Godlevsky V V and Rabe K M 2001 *Phys. Rev. B* **63** 134407
[32] Vitos L 2007 *Computational Quantum Mechanics for Materials Engineers* (London: Springer-Verlag)
[33] Andersen O K, Jepsen O and Krier G 1994 *Lectures on Methods of Electronic Structure Calculations* (Singapore: World Scientific) pp. 63–124
[34] Vitos L, Skriver H L, Johansson B and Kollár J 2000 *Comput. Mater. Sci.* **18** 24
[35] Vitos L 2001 *Phys. Rev. B* **64** 014107
[36] Zwierzycki M and Andersen O K 2009 *Acta Phys. Pol. A* **115** 64
[37] Kollár J, Vitos L and Skriver H L 2000 *Electronic Structure and Physical Properties of Solids: The Uses of the LMTO Method* (Berlin: Springer-Verlag) p. 85
[38] Soven P 1967 *Phys. Rev.* **156** 809
[39] Vitos L, Abrikosov I A and Johansson B 2001 *Phys. Rev. Lett.* **87** 156401
[40] Györffy B L 1972 *Phys. Rev. B* **5** 2382
[41] Vitos L, Korzhavyi P A and Johansson B 2003 *Nat. Mater.* **2** 25
[42] Kim D Y, Hong J and Vitos L 2014 *Phys. Rev. B* **90** 144413
[43] Li C M, Yang R, Johansson B and Vitos L 2016 *Phys. Rev. B* **94** 214108
[44] Li C M, Hu Y F, Feng W J and Huang R Z 2018 *Phys. Rev. B* **98** 224107
[45] Li C M, Zhang Y, Feng W J, Huang R Z and Gao M 2020 *Phys. Rev. B* **101** 054106
[46] Perdew J P, Burke K and Ernzerhof M 1996 *Phys. Rev. Lett.* **77** 3865
[47] Moruzzi V L, Janak J F and Schwarz K 1988 *Phys. Rev. B* **37** 790
[48] Li C M, Hu Q M, Yang R, Johansson B and Vitos L 2010 *Phys. Rev. B* **82** 094201
[49] Skubic B, Hellsvik J, Nordström L and Eriksson O 2008 *J. Phys.: Condens. Matter* **20** 315203
[50] Antropov V P, Katsnelson M I, Harmon B N, Schilfgaarde M van and Kusnezov D 1996 *Phys. Rev. B* **54** 1019
[51] García-Palacios J L and Lázaro F J 1997 *Phys. Rev. B* **55** 1006
[52] Watson R E, Blume M and Vineyard G H 1969 *Phys. Rev.* **181** 811
[53] Bergman A, Taroni A, Bergqvist L, Hellsvik J, Hjörvarsson B and Eriksson O 2010 *Phys. Rev. B* **81** 144416
[54] Liechtenstein A, Katsnelson M I and Gubanov V A 1984 *J. Phys. F: Met. Phys.* **14** L125
[55] Liechtenstein A, Katsnelson M I, Antropov V P and Gubanov V A 1987 *J. Magn. Magn. Mater.* **67** 65
[56] Staunton J, Gyöffy B L, Pindor A J, Stocks G M and Winter H 1984 *J. Magn. Magn. Mater.* **45** 15
[57] Dutta B, Bhandary S, Ghosh S and Sanyal B 2012 *Phys. Rev. B* **86** 024419
[58] Steinle-Neumann G, Stixrude L and Cohen R E 1999 *Phys. Rev. B* **60** 791
[59] Buschow K H J, Engen P G van and Jongebreur R 1983 *J. Magn. Magn. Mater.* **38** 1
[60] Umetsu R Y, Kobayashi K, Kainuma R, Fujita A and Fukamichi K 2004 *Appl. Phys. Lett.* **85** 2011
[61] Umetsu R Y, Kobayashi K, Kainuma R, Yamaguchi Y, Ohoyama K, Sakuma A and Ishida K 2010 *J. Alloys Compd.* **499** 1
[62] Hamad B 2014 *J. Appl. Phys.* **115** 113905

[63] Ram S, Chauhan M R, Agarwal K and Kanchana V 2011 *Phil. Mag. Lett.* **91** 545
[64] Schroeder K, Waybright J, Kharel P, Zhang W, Valloppilly S, Herran J, Lukashev P, Huh Y, Skomski R and Sellmyer D J 2018 *AIP Adv.* **8** 056431
[65] Buschow K H J and Engen P G van 1981 *J. Magn. Magn. Mater.* **25** 90
[66] Kanomata T, Chieda Y, Endo K, Okada H, Nagasako M, Kobayashi K, Kainuma R, Umetsu R Y, Takahashi H, Furutani Y, Nishihara H, Abe K, Miura Y and Shirai M 2010 *Phys. Rev. B* **82** 144415
[67] Webster P J and Ziebeck K R A 1973 *J. Phys. Chem. Solid.* **34** 1647
[68] Bentouaf A, Mebsout R and Aïssa B 2019 *J. Alloys Compd.* **771** 1062
[69] Faure P, Deslandes B, Bazin D, Tailland C, Doukhan R, Fournier J M and Falanga A 1996 *J. Alloys Compd.* **244** 131
[70] Webster P J, Ziebeck K R A, Town S L and Peak M S 1984 *Philos. Mag. B* **49** 295
[71] Punkkinen M P J, Kwon S K, Kollár J, Johansson B and Vitos L 2011 *Phys. Rev. Lett.* **106** 057202
[72] Roy T, Pandey D and Chakrabarti A 2016 *Phys. Rev. B* **93** 184102